Available online at www.sciencedirect.com
ScienceDirect
Catalysis Today 120 (2007) 426–431
CATALYSIS TODAY
www.elsevier.com/locate/cattod

Intrinsic linear scaling of hydrogen storage capacity of carbon nanotubes with the specific surface area

Renju Zacharia, Keun Young Kim, Sang Woon Hwang, Kee Suk Nahm *

Nanomaterial Research Center and School of Chemical Engineering and Technology, Chonbuk National University, Chonju 561-756, Republic of Korea

Available online 7 November 2006

Abstract

The linear scaling of the gravimetric hydrogen storage capacity of single- and multi-walled carbon nanotubes (SWNTs and MWNTs) with the specific surface area is investigated at ambient temperature (298 K) and technically relevant pressures (0.9–1.6 MPa). All samples are found to adsorb hydrogen reversibly and their adsorption exhibits type-II BET isotherms according to the IUPAC classification. While there is strong sample-dependency on their pressure–composition isotherms, all of them follow the Henry's Law in the pressure range under consideration. A comparison of the observed slope of specific surface area *versus* gravimetric storage capacity with that of a theoretically predicted one using a hypothetical condensation model and that of chemically modified carbon nanotubes revealed that the hydrogen storage capacity depends on the accessibility of internal surfaces of nanostructured carbon. The linear scaling of hydrogen storage capacity with the respective specific surface area suggests that the hydrogen adsorption in carbon nanotubes depends on the specific surface area and is irrespective of the type of the nanotubes that is used.

Keywords: Hydrogen storage; Adsorption isotherm; Sievert method; Specific surface area; Linear scaling

1. Introduction

Adsorption of hydrogen in carbon nanotubes (CNTs) is envisaged as one of the most promising methods of storing hydrogen for on-board applications [1,2]. At ambient temperature and pressure conditions, adsorption of hydrogen by CNTs is predominantly physisorption, where the dominant mechanism arises from the weak van der Waals type of interactions between hydrogen molecules and nanotube walls [3,4]. At sub-critical temperatures, the magnitude of this interaction becomes stronger when compared with the thermal motion of the gas molecules. The adsorption of hydrogen on carbon nanotubes in this regime can be addressed using a simple condensation model [4]. It has been demonstrated that, within this model, the hydrogen storage capacity of nanostructured carbon materials is proportional to the specific surface area (SSA) of the material. Under this storage conditions, the prototypical two-dimensional basal plane of graphite with a maximum surface area (with both sides included) of 2630 $m^2 g^{-1}$ can store hydrogen up to 3.3 wt.% [4]. However, this model does not explicitly accommodate the effect of temperature on the hydrogen storage capacity and therefore, it tends to overestimate the storage capacity at ambient temperature. This is so, because at ambient temperature, the thermal motions of gas molecules exceed the interaction of hydrogen with carbon nanotube surfaces [4]. Nevertheless, the model provides the limiting hydrogen storage capacity as a function of the specific surface area of the nanotube samples. In the recent times, some experiments have been performed to unravel the dependence of the gravimetric hydrogen storage capacities of carbon materials with the respective specific surface area [5–7]. Such studies are done with a view to improve the maximum storage capacities of nanostructured carbon materials by understanding its dependence of SSA. These studies suggest that, depending on the types of materials used, the specific surface area shows a characteristic slope typically much less than the theoretical maximum predicted using the condensation model [6,7]. However, these experiments are mostly carried out at cryogenic temperatures. As the hydrogen storage capacity of carbon nanomaterials do not show

* Corresponding author. Tel.: +82 63 270 2311; fax: +82 63 270 2306.
E-mail address: nahmks@chonbuk.ac.kr (K.S. Nahm).

0920-5861/$ – see front matter
doi:10.1016/j.cattod.2006.09.026

linear temperature dependence, the data collected at cryogenic temperature poses difficulties in predicting the SSA dependence at the temperatures relevant for practical applications [8].

In this work, we present the hydrogen storage characteristics of three different samples of carbon nanotubes (SWNTs and MWNTs) under ambient temperature (298 K) and pressures (0.9–1.6 MPa) and correlate the maximum hydrogen storage capacity with their specific surface area. The nitrogen adsorption characteristics of these samples at 77 K can be described using Langmuir or BET adsorption isotherm depending on the equilibrium pressure. The pressure–composition isotherms of the samples measured at 298 K show significant sample-dependency. However, in the pressure range considered in our studies, all of them can be fitted using the Henry's Law. A comparison of the observed dependence of the gravimetric hydrogen storage capacities with the theoretical maximum hydrogen storage capacity predicted using a hypothetical condensation model and that of chemically modified carbon nanotubes is made to understand effect of the storage temperature and the available surface area on the hydrogen storage capacity of our samples.

2. Experimental

Two batches of purified nanotube samples were obtained from CNT Corporation Ltd., and the Hanyang University. The former (sample 1) consisted mainly of multi-walled carbon nanotubes (MWNTs) with a typical diameter distribution of 10 to 40 nm. The latter (sample 2) consisted mostly of single walled carbon nanotubes (SWNTs), and has diameter varying from 1 to 10 nm. The samples 1 and 2 are synthesized via chemical vapor deposition and have a purity of 95%. The residual metals present in these samples include traces of iron, aluminum, cobalt and nickel, as documented by the suppliers. These commercial samples were used with out further purification. Another sample of carbon nanotubes (MWNTs, sample 3) was synthesized in our laboratory via rapid thermal chemical vapor deposition (RTCVD) of acetylene precursor also used in our study. The as-produced specimens of sample 3 were purified using standard procedure involving acid treatment, and vacuum annealing to remove catalyst metal particles and amorphous carbon deposits [9]. Thermogravimetric analysis of this sample has been reported previously, indicates that the sample has residual metal content, less than 2–3% [9]. According to previous results, it also contains minute quantities of amorphous carbon [9]. The Raman spectra and the TEM analysis of the samples were measured using a Microraman spectrometer (RENISHAW) and transmission electron microscope (JEOL JEM 2010), respectively.

Brinauer–Emmet–Teller (BET) adsorption studies and surface characterizations of the samples were performed by N_2 adsorption at 77.3 K using static multipoint technique in a commercial volumetric adsorption analyzer (ASAP 2000) from micrometrics. Prior to adsorption studies, known quantities of samples were outgassed for 24 h at 673 K. Outgassed samples were cooled down to 77.3 K and were exposed to known amounts of nitrogen admitted into the reactor cell in a stepwise manner. Isotherms are plotted as volumes of N_2 adsorbed at STP as a function of relative pressure (P/P_0). The volumes are then converted to the number of moles of gas adsorbed using the equation of the state of an ideal gas.

Isothermal hydrogen storage capacity measurements were performed in a Sievert's type of volumetric device. It consisted of a hydrogen buffer-tank, which was connected to the reactor and a high sensitive and calibrated pressure transducer (0.05% error at full-scale). The dead volume of the system was determined using the iterative Redlich–Kwong equation of the state of helium gas [10]. The reactor volume was subsequently determined by the helium-displacement method, where the volume calculations were performed using the equation of state of an ideal gas. The determined volume was further cross-checked using the hydrogen adsorption data of a known amount of the intermetallic alloy $LaNi_5$ [11]. Nearly 0.1 g of carbon nanotube sample was used in each hydrogen storage study. Prior to each storage experiment, the nanotube samples were outgassed for nearly 6 h by heating to 400 °C under continuous evacuation up to 10^{-4} Torr. The degassing was typically performed until a constant and reproducible background pressure was obtained. For adsorption experiments high purity hydrogen gas (99.999%) was admitted into the buffer and maintained until the equilibrium was established. The initial equilibrium pressure of hydrogen in the buffer was maintained constant around 3 MPa for all experiments. After attaining the equilibrium, the gas was isothermally vented into the reactor and the pressure drop in the hydrogen gas was measured as a function of time. The final equilibrium pressure in a typical adsorption experiment was found to be around 1.5 MPa. The gravimetric storage capacity of nanotube samples was determined from the pressure drop of hydrogen using ideal gas equation. For each sample, pressure–composition isotherms were obtained by performing hydrogen storage at various equilibrium pressures. All adsorption experiments were carried out at 298 K. Further details of the hydrogen storage measurement can be obtained elsewhere [12].

3. Results and discussions

3.1. Structural characterization

Representative TEM images of carbon nanotubes samples are displayed in Fig. 1, where panels (a) and (b) correspond to the samples 2 and 3, respectively. The commercial sample obtained from CNT Corporation Ltd., contains MWNTs with the outer diameter ranges from 10 to 40 nm. Sample 2 mostly is SWNTs with a typical diameter of 10 nm while the sample 3 is predominantly MWNTs with approximately 10 nm diameter. On an average, they have between 8 and 10 shells. In Fig. 2, the Raman spectra of three samples are displayed. The Raman spectra of the nanotube samples display two strong peaks localized at and 1350 and 1580 cm^{-1}. The band appearing at 1350 cm^{-1} arises due to chemically induced disruption of hexagonal carbon order in the carbon nanotube walls [13]. The bands that appear at 1580 cm^{-1} arise due to the tangential vibration of carbon atoms along the tube axis (G^+) and along the

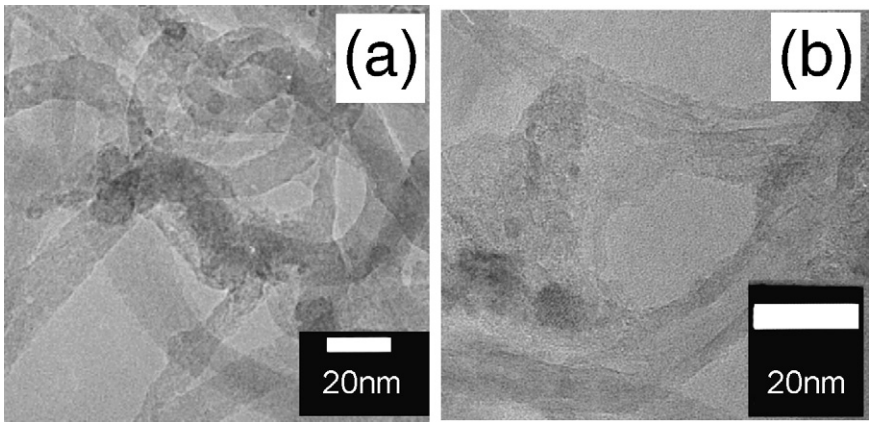

Fig. 1. Transmission electron microscopy images of sample 2 (a) and sample 3 (b) carbon nanotubes. Sample 2 consist mainly of SWNTs while sample 3 contains mostly.

circumferential direction (G^-) with displacement modes A_{1g}, E_{1g} and E_{2g}. Estimated value of the ratio of intensity of disordered and graphitic peaks (I_D/I_G) are found to be 0.79, 0.37 and 0.38, respectively, for samples 1, 2 and 3. These values suggest that the non-graphitic carbon contents in samples 2 and 3 are negligible [13]. On the other hand, the sample obtained from CNT Corporation Ltd., has substantial quantity of amorphous carbon. An interesting feature that can be noted on the lower energy side of graphitic peaks of the sample 3 is the considerable enhancement of the intensities originating from the Breit–Wigner–Fano resonance. This resonance arises due to the agglomeration of SWNTs to form the so-called nanotube bundles that generally happens when the nanotubes are treated with acids [14].

3.2. Langmuir and BET adsorption isotherms and determination of specific surface area

3.2.1. Langmuir model

Langmuir model describes the adsorption of nitrogen on carbon materials near sub-critical temperatures. The Langmuir adsorption isotherm is a monotonically increasing function of pressure, which saturates at the monolayer capacity, n_m. It can be put in the form [15]:

$$\frac{P}{n} = \frac{1}{bn_m} + \frac{P}{n_m} \tag{1}$$

The monolayer capacity and the coefficient, b can be extracted from a simple linear fit of the data. In Fig. 3(a)–(c), we present the plots of P/v *versus* P for samples 1, 2 and 3, respectively. Very good fit is observed in the low-pressure region (<0.2 MPa). However, strong deviation from the linearity is observed with the increase in pressure. This deviation can be attributed to the presence of excess adsorption maximum, which cannot be accurately described using the Langmuir model. The deviation found at the onset of high pressures corresponds to the completion of the monolayer. Since the Langmuir model of adsorption is valid only where the slope b is the maximum we make the linear fit to the data in the low-pressure region to extract n_m and b. The monolayer capacity is used to determine the Langmuir surface area (Σ_L) using the relation: $\Sigma_L = n_m \sigma N_0$, where σ and N_0 are the area of the hydrogen molecule and N_0. The values of σ are typically obtained from the monolayer capacity of hydrogen on a graphene sheet. The estimated values of Σ_L are displayed in Table 1.

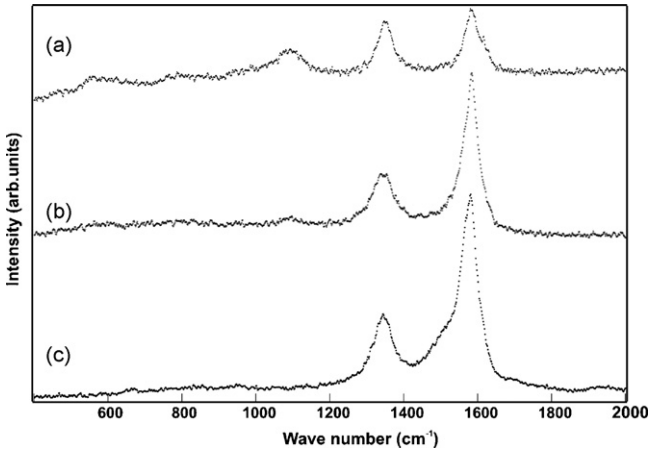

Fig. 2. Raman spectra of carbon nanotubes (a) sample 1, (b) sample 2 and (c) sample 3 recorded using an excitation wavelength of 1064 nm.

3.2.2. BET adsorption isotherm

Adsorption of nitrogen in carbon materials at high pressure can be modeled more accurately using multilayer adsorption model proposed by Brauner, Emmet and Teller. This model is based on the detailed balancing of adsorption and desorption, where the dependence of number of moles of gas adsorbed on the relative pressure is given by [15]:

$$\frac{1}{n[(P_0/P) - 1]} = \frac{i}{cn_m} + \frac{c-1}{cn_m}\frac{P}{P_0} \tag{2}$$

Fig. 4 shows the BET adsorption isotherms of samples 1–3. All samples exhibit an initial steep rise in the adsorption characteristics of a type-II isotherm according to the IUPAC classification [15]. Type-II adsorption characteristics of raw and purified

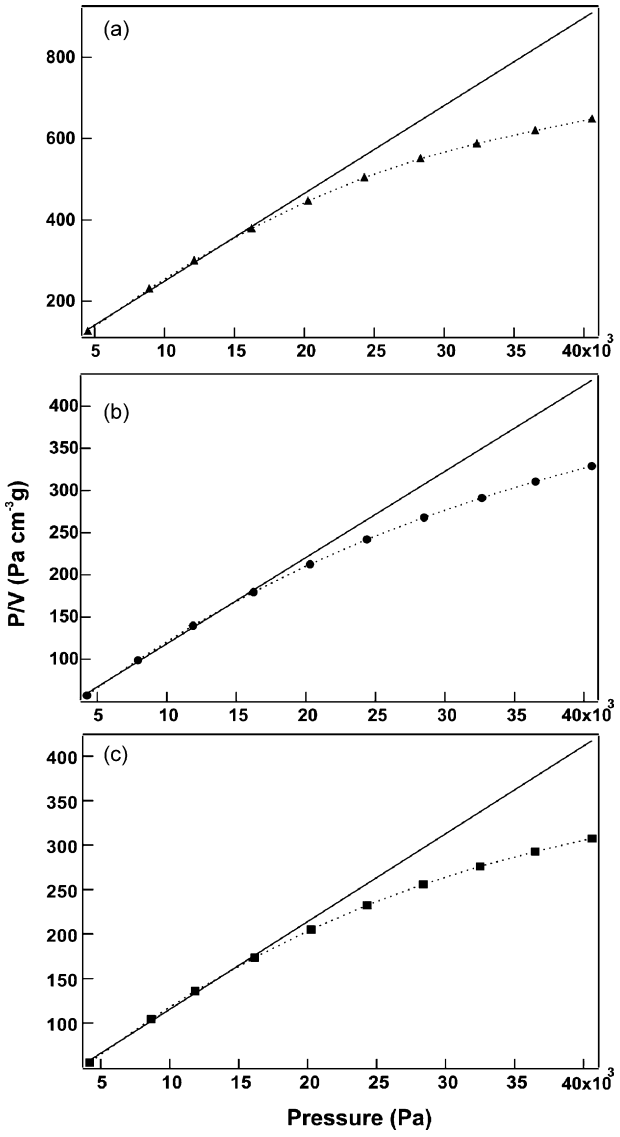

Fig. 3. The Langmuir adsorption plots (P/V *vs.* P) of samples 1 (a), 2 (b) and 3 (c) measured using nitrogen adsorption at 77.3 K.

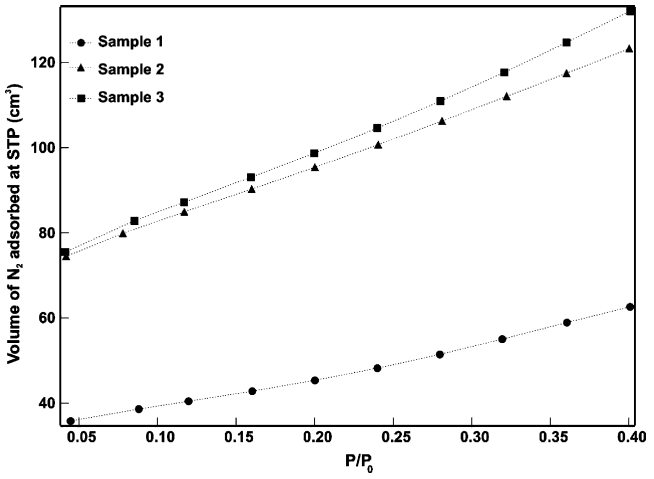

Fig. 4. The BET adsorption isotherms of samples 1–3 measured using nitrogen adsorption in the relative pressure range 0–0.6.

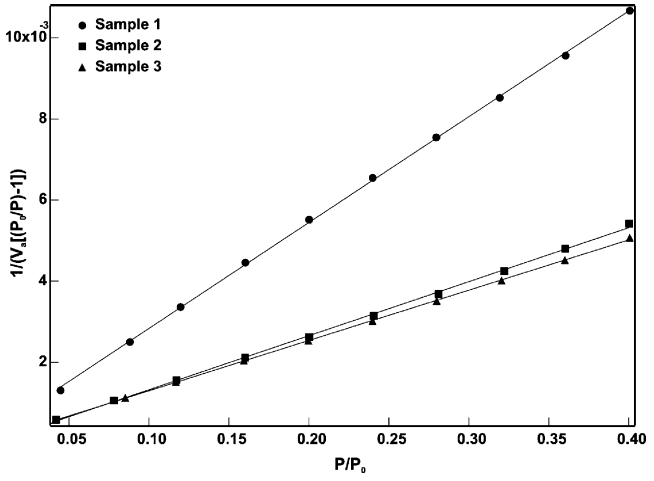

Fig. 5. Plot of $1/V_a[(P_0/P) - 1]$ *vs.* P/P_0 using the BET data showing the linear fit in the relative pressure range 0–0.6.

carbon nanotubes recorded in previous studies show similar characteristics [16,17]. The steep increase in the adsorption is attributed to the filling of micropores [17]. The greater accuracy of BET model in fitting the experimental adsorption data, especially at higher pressures is evident in Fig. 5 which contains the plot of $1/[V_a(P_0/P) - 1]$ *versus* P/P_0 for all three samples. As previously mentioned, the measured volumes are converted into the number of moles of gas adsorbed using the equality: $n_m/n = v_m/v$, where n and v correspond to the measured number of moles and the volume of nitrogen adsorbed. The slope and the intercept of these plots are obtained via simple linear regression, according to Eq. (2) and are used to compute the BET specific surface area, Σ_{BET}. The latter is calculated using the dependence $\Sigma_{BET} = n_m \sigma N_0$. Here, the area of nitrogen molecule (16.2 Å^2) can be used as σ due to the excellent fit observed in the higher pressure region which stems from the accuracy of BET model in describing the multilayer adsorption. The calculated values of Σ_{BET} are presented in Table 1. It can be seen that both the Langmuir surface area and BET surface area increase in the order sample 1 < sample 2 < sample 3.

Table 1
Surface area and hydrogen storage capacities of carbon nanotubes samples measured at 298 K and an equilibrium pressure of around 1.6 MPa

Sample ID	Σ_L ($m^2\ g^{-1}$)	Σ_{BET} ($m^2\ g^{-1}$)	wt.% (observed)	wt.% (condensation model)
Sample 1	176.2	165.4	0.07	0.42
Sample 2	373.2	327.5	0.15	0.84
Sample 3	386.5	349.4	0.16	0.89

3.3. Hydrogen storage properties

3.3.1. Transient hydrogen storage studies

We begin our discussion on the gravimetric hydrogen storage capacities of carbon nanotubes by referring to Fig. 6, which contains the transient hydrogen adsorption profiles of samples 1–3. The profiles correspond to the adsorption of hydrogen during an exposure at ambient temperature (298 K) and an initial pressure of 3 MPa. The final pressure after reaching the equilibrium is found to be nearly 1.6 MPa. Here, the fall in the pressure can be attributed to two factors: the isothermal expansion of hydrogen and adsorption of hydrogen on carbon nanotube surfaces. We determine the pressure reduction owing to the isothermal expansion of hydrogen using the van der Waals equation. The number of moles of hydrogen adsorbed is hence computed using the fall in pressure due to the hydrogen adsorption. In each case, the gravimetric storage capacity is determined using the expression: $Wt_H/(Wt_H + Wt_{CNT}) \times 100$, where Wt_H and Wt_{CNT} correspond to the weight of hydrogen adsorbed and weight of carbon nanotube samples. The maximum hydrogen storage capacities of samples 1, 2, and 3 are 0.07, 0.15 and 0.16 wt.%, respectively. The reversible hydrogen storage capacity is further confirmed by the re-adsorption studies, where previously exposed samples are re-exposed to hydrogen only after room temperature outgassing [12]. Upon re-adsorption all samples stored almost 95–100% of its initial hydrogen uptake as evident from the re-adsorption profiles provided in the inset of Fig. 6.

3.3.2. Pressure–composition isotherms

In this section we present our results on the pressure–composition isotherms of all samples measured at 298 K in the equilibrium pressure range of 0.9–1.6 MPa. In Fig. 7, the isotherms (a), (b) and (c) correspond to the pressure–composition profiles of samples 1, 2 and 3, respectively. It can be observed that the pressure–composition isotherm of sample 1 shows a linear variation in the beginning and then shows a tendency to saturate, while both samples 2 and 3 exhibit a linear variation in the pressure range studied. This linear behavior can be explained on the basis of the Henry's Law [8,15]. Although the data presented here are not statistically significant, a similar compliance of the pressure–composition isotherms with the Henry's Law has been previously noted by Rzepka et al., in the low-pressure region (<3 MPa), which substantiates our conclusions [8].

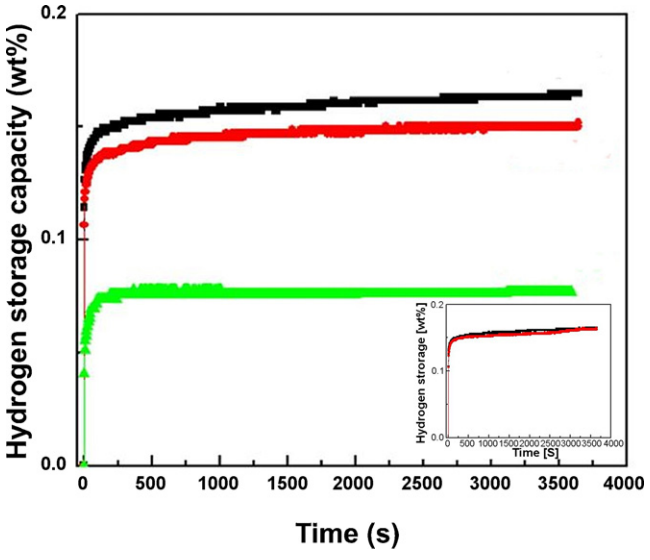

Fig. 6. Transient hydrogen adsorption profiles of carbon nanotubes measured at room temperature (298 K) and an equilibrium pressure of 1.6 MPa. The green, red and black traces, respectively, indicate the profiles for samples 1, 2 and 3. In the inset the hydrogen re-adsorption profile for sample 3 is displayed. The black trace corresponds to the initial hydrogen adsorption data. The red one indicates the hydrogen adsorption after the room temperature degassing. (For interpretation of the references to colour in this figure legend, the reader is referred to the web version of the article.)

3.3.3. Linear scaling of hydrogen storage capacity with specific surface area

In order to evaluate the dependence of specific surface area, we used the BET specific surface area (Σ_{BET}) as mentioned in Section 3.2. They are 165, 327 and 349 $m^2\ g^{-1}$, respectively, for samples 1, 2 and 3. Also, we utilized the maximum reversible hydrogen storage capacity recorded at 1.6 MPa and 298 K, which are displayed in Table 1. The linear scaling of gravimetric hydrogen storage capacity with BET surface area is displayed in Fig. 8. In the following, we try to compare the observed gravimetric storage capacity with the theoretical maximum hydrogen storage capacity obtained using a hypothetical condensation model [4]. In this model, the condensation of one monolayer of hydrogen on a graphene layer can be expressed as the ratio of the specific surface area and the area occupied single hydrogen molecule:

$$\frac{\mathrm{Wt}(H_2)}{\mathrm{Wt}(C)} = \frac{\Sigma_{BET} M_{H_2}}{\sigma N_0} \tag{3}$$

Here, M_{H_2} and σ are the mass and area of hydrogen molecule while N_0 is the Avogadro number. From the ratio of mass of hydrogen to carbon, we find the theoretical maximum

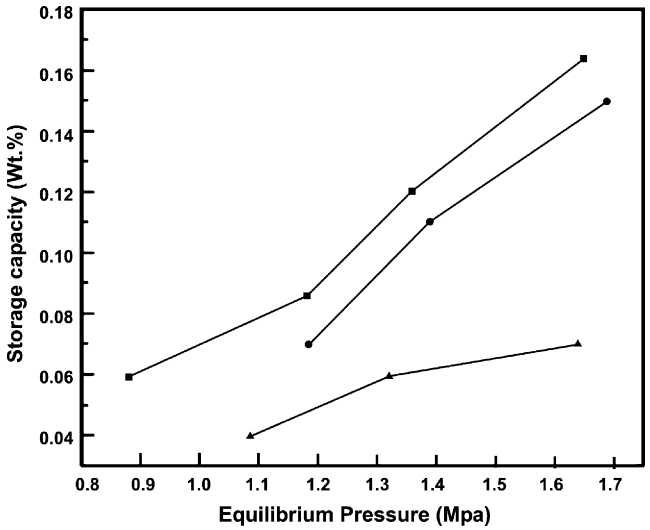

Fig. 7. Linear increase in the hydrogen storage capacities of carbon nanotube samples with equilibrium pressure in the range 0.9–1.6 MPa, obtained at room temperature. In the figure, samples 1 (▲), 2 (●), and 3 (■) are presented. The profiles follow Henry's Law in this pressure region.

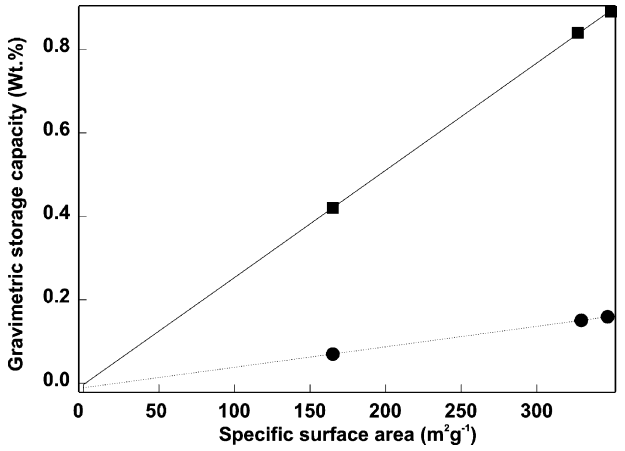

Fig. 8. The linear scaling of the gravimetric hydrogen storage capacity of carbon nanotubes with the specific surface area. In the figure, trace (■) which indicates the ideal hydrogen storage capacity obtained using the empirical condensation model is compared with the experimental data (●).

gravimetric storage capacity $(Wt_H/(Wt_H + Wt_{CNT}) \times 100)$ corresponding to the experimentally determined BET surface area. In Fig. 8, we compare the experimentally observed (●) and theoretically estimated hydrogen storage capacities (■) as functions of specific surface area. From the fit to the experimental data, we found that the linear scaling of hydrogen storage capacity can be accounted using the condensation model. Nevertheless, only about 16% of the predicted storage capacity is fulfilled in our adsorption experiments. Note that the model assumes the condensation of hydrogen at 273 K even though the critical temperature is around 33 K. This, therefore, overestimates the room temperature hydrogen storage in carbon nanotubes. However, a part of the mismatch also due to surfaces of carbon nanotubes inaccessible to carbon nanotubes. To understand this contribution, we qualitatively compare the slope of the fit of our data (4.9×10^{-4} wt.%/m^2 g^{-1}) with the data measured by Ansón et al. for nanotube samples at 298 K [18]. They obtained a maximum hydrogen storage capacity of 0.02 wt.% at 298 K for chemically activated CNTs and there is only negligible influence of SSA on the hydrogen storage capacity. We assume that this partially arises from the chemical modification of the samples. Therefore, it can be concluded that the availability of high surface area is not the single criterion for the enhanced hydrogen storage capacity of carbon nanotubes, but accessibility of all surfaces at experimental conditions remains essential to when practical hydrogen storage applications are considered.

4. Conclusions

In conclusion, we investigated the dependency of the gravimetric hydrogen storage capacity of single- and multi-walled carbon nanotubes (SWNTs and MWNTs) with the specific surface area. We found that the storage capacity measured at 298 K and an equilibrium pressure of 1.6 MPa scales linearly with the SSA, irrespective of the type of nanotubes used. These samples adsorb hydrogen reversibly and their pressure–composition isotherms follow Henry's Law in the pressure range considered. Comparison of the SSA dependency of hydrogen storage capacity of graphene sheets obtained from a condensation model and chemically modified CNTs suggests that the hydrogen storage capacity of nanotubes depends not only on the high specific surface area but also on the accessibility of the internal surfaces.

Acknowledgments

This study was supported by ''National RD&D Organization for Hydrogen & Fuel Cell'' and ''Ministry of Commerce, Industry and Energy''.

References

[1] R.G. Ding, J.J. Finnerty, Z.H. Zhu, Z.F. Yan, G.Q. Lu, in: H.S. Nalwa (Ed.), Encyclopedia of Nanoscience and Nanotechnology, American Scientific Publishers, 2004.
[2] F.L. Darkrim, P. Malbrunot, G.P. Tartaglia, Int. J. Hydrogen Energy 27 (2002) 193.
[3] K.A. Williams, P.C. Eklund, Chem. Phys. Lett. 320 (2000) 352.
[4] A. Zuttel, P. Sudan, Ph. Mauron, T. Kiyobayashi, Ch. Emmenegger, L. Schlapbach, Int. J. Hydrogen Energy 27 (2002) 203.
[5] B. Panella, M. Hirscher, S. Roth, Carbon 34 (2005) 2209.
[6] A. Zuttel, P. Wenger, P. Sudan, P. Mauron, S. Orimo, Mater. Sci. Eng. B 108 (2004) 9.
[7] H.G. Schimmel, G. Nijkamp, G.J. Kearley, A. Rivera, K.P. de Jong, F.M. Mulder, Mater. Sci. Eng. B 108 (2004) 124.
[8] M. Rzepka, P. Lamp, M.A. de la Casa-Lillo, J. Phys. Chem. B 102 (1998) 10894.
[9] A.K.M.F. Kibria, Md. Shajahan, Y.H. Mo, M.J. Kim, K.S. Nahm, Diamond Relat. Mater. 13 (2004) 1865.
[10] C. Zhang, X. Lu, A. Gu, Int. J. Hydrogen Energy 29 (2004) 1271.
[11] G. Liang, J. Hout, R. Schulz, J. Alloys Compd. 320 (2001) 133.
[12] R. Zacharia, K.Y. Kim, A.K.M.F. Kibria, K.S. Nahm, Chem. Phys. Lett. 412 (2005) 369.
[13] A. Jorio, M.A. Pimenta, A.G. Souza Filho, R. Saito, G. Dresselhaus, M.S. Dresselhaus, New J. Phys. 5 (2003) 139.
[14] C. Jiang, K. Kempa, J. Zhao, U. Schlecht, U. Kolb, T. Basche, M. Burghard, A. Mews, Phys. Rev. B 66 (2002) 161404.
[15] A.W. Adamson, Physical Chemistry of Surfaces, John Wiley & Sons, New York, 1990.
[16] F. Li, Y. Wang, D. Wang, F. Wei, Carbon 42 (2004) 2375.
[17] M. Eswaramoorthy, R. Sen, C.N.R. Rao, Chem. Phys. Lett. 304 (1999) 207.
[18] A. Ansón, J. Jagiello, J.B. Parra, M.L. Sanjuán, A.M. Benito, W.K. Maser, M.T. Martínez, J. Phys. Chem. B 108 (2004) 15820.